DOI 10.1007/s10511-024-09828-z
Astrophysics, Vol. 67, No. 2, August, 2024

RECONSTRUCTION OF THE QUINTESSENCE DARK ENERGY POTENTIAL FROM A GAUSSIAN PROCESS

E. Elizalde[1], M. Khurshudyan[1], K. Myrzakulov[2,3], and S. Bekov[2,3]

This paper presents the reconstruction of the quintessence dark energy potential in a model- independent way. Reconstruction relies on a Gaussian process and on available expansion rate data. Specifically, 40-point values of $H(z)$ are used, consisting of a 30-point sample deduced from a differential age method and an additional 10-point sample obtained from the radial BAO method. Results are obtained for two kernel functions and for three different values of H_0. This sheds light on the H_0 tension problem indicating that it is not just a numerical problem. The model-independent reconstruction of the potential can serve as a reference to constraint available models and construct new ones. Various possibilities, including $V(\phi) \sim e^{-\lambda\phi}$, are compared with the reconstructions here obtained, which is notably the first truly model-independent reconstruction of the quintessence dark energy potential. This allows the selection of new models that can be interesting for cosmology. The method can be extended to reconstruct the potential of related dark energy models, to be considered in future work.

Keywords: *quintessence dark energy: potential: Gaussian process*

1. Introduction

Modern cosmology often clearly reflects how our previous knowledge of the Universe needs to be modified to accommodate new observations. The H_0 tension problem is one of those pointing out a huge difference between

[1] Consejo Superior de Investigaciones Científicas, ICE/CSIC-IEEC, Campus UAB, Carrer de Can Magrans s/n, 08193 Bellaterra (Barcelona), Spain, e-mail: martiros.khurshudyan@csic.es
[2] Eurasian National University, Nur-Sultan 010008, Kazakhstan
[3] Ratbay Myrzakulov Eurasian International Centre for Theoretical Physics, Nur-Sultan 010009, Kazakhstan

Published in Astrofizika, Vol. 67, No. 2, pp. 205-227 (May 2024). Original article submitted June 10, 2024.

the early time and late time measurements of the Hubble constant H_0 [1,2]. Various interesting proposals on how the problem could be solved have appeared in the literature, such as [3-16] (and references therein). In the last several years, we have witnessed significant technological developments helping us to improve the data collection and analysis process by orders of magnitude. But without the possibility of doing direct experiments with the Universe, it is still difficult to deal with some problems. Why could we not make significant progress in solving some long-standing problems? Is it because of an issue with our understanding of what data mean? Eventually, is there a problem with the model-construction strategies to reflect our understanding of what the observational data say? Could this reflect that we cannot avoid a bias when we link a model with the data? There is a solid belief, that Machine Learning (ML) eventually will answer a huge part of the above-mentioned questions. But, what exactly it does and why is it nowadays one of the top research fields? ML tries to do the following: it does not start from questions but, on the contrary, having the answers finds the questions (the models) explaining what we have in terms of experimental data. It sounds unusual and requires significant effort to understand how and why it works. Recent attempts to use such tools in physics (and not only in physics) have proven to be very promising.

Our paper is aimed to study a specific dark energy model in a model-independent way by using the advantages of a specific ML approach [17-39] (see references therein for additional discussion on different developments concerning dark energy models and related problems). In particular, we will study a quintessence dark energy when a Gaussian Process (GP) is involved (see for instance [40,41] covering some discussion about quintessence dark energy models). GPs provide interesting departures from standard reasoning in various fields. Their recent applications to cosmology showed very interesting departures not reported previously (see [42-52] and references therein). The reconstruction of $f(T)$ gravity from the expansion rate data, allowing us to obtain very tight constraints on the model parameters of some popular $f(T)$ models is among them [42]. Moreover, a recent paper by two of the authors has shown how GPs can be used to tackle the Swampland criteria for dark energy dominated Universe in a model-independent way [43]. In particular, it has been demonstrated there that the expansion rate data can be used, instead of assuming a specific form for the potential describing the quintessence dark energy, to tackle the Swampland criteria. In other words, the whole analysis is based on the expansion rate data allowing the exploration of the features, which in some sense could be biased due to the use of a specific dark energy model. In this way, a hint indicating that the Swampland criteria in its recent form is not suitable for a dark energy-dominated Universe has been found. Among other interesting results, it was found that an effective theory being in the Swampland could (or not) end up there. Moreover, starting out of the Swampland it is possible to end up either inside or outside of it. Having such interesting results in our hands, probably it would be possible in the near future to have unsuspected departures from the standard reasoning about effective field theories (EFT) which is a promising task to be tackled yet. The fact that ML is designed to find the questions from the answers gives hope that, in the near future, some interesting developments in this direction may arise. We would like to mention that there is another interesting approach, known as Bayesian Machine Learning, which we hope can eventually be very efficient in overcoming such limitations too [4,10,11] (see there how it can be used to tackle the H_0 tension problem).

Now, let us come back to [43] where no specific form for the potential has been used. However, it is easy to

see that the reconstruction of the quintessence dark energy potential itself is possible too, allowing also to obtain the constraints on the existing models. Moreover, it can be used to craft new models and gain some hints about how, for instance, the H_0 tension problem can be solved in a quintessence dark-energy dominated Universe. In this way, we can indicate that the results of that paper provide a unique possibility to treat quintessence dark energy models, too, since the most model-independent reconstruction of the general picture has been obtained. Motivated by this possibility, given by the use of GPs, the potential was reconstructed, in a model-independent way from available expansion rate data, and, in addition, a new viable quintessence dark energy model was obtained. In particular, based on the mean of the obtained reconstructions, the potential $V(\phi) \sim \phi^{\lambda}\left[1-\sin^{n}(\beta\phi)\right]$ has been proposed as a new form of quintessence dark energy-up to our best knowledge this potential has not been discussed anywhere previously. Other models were also considered, as $V(\phi) \sim \phi^{\lambda}$, $V(\phi) \sim \phi^{\lambda}\left[1-\cos\left(\beta\phi^{n}\right)\right]$ and $V(\phi) \sim e^{-\lambda\phi}$ (see for instance [53] and references therein) and values of the model's parameters were estimated, indicating when they could be 1) viable and interesting for cosmology, and 2) used to solve the H_0 tension problem.

To end this section, we would like to mention also that, in our analysis here, we will use two kernels and consider three different cases for the value of the parameter H_0. In this way, hints are given about the forms and constraints on the quintessence dark energy models that could be very useful in understanding how the H_0 tension problem could be alleviated. We do hope that these new results combined with the results discussed in [43] will lead to new developments in future studies of quintessence dark energy models. It should be mentioned that [43] already contains a discussion about different aspects of the quintessence Universe, therefore, here we will not reproduce them again.

This paper is organized as follows. The description of the GP is discussed in Sect. 2. In the same section, we present the details of the potential reconstruction process. The main results are discussed in Sect. 3, which is followed by an analysis of their implications. The final conclusions of the analysis are given in Sect. 4.

2. The method and the model

The goal of this work is to provide a model-independent reconstruction of the quintessence dark energy potential by using a GP. We will present some details of how this can be achieved. We shall start from the background dynamics demonstrating what are the steps to follow to make the GP work, while some discussion on the GP itself will be presented at the end of this section.

We consider General Relativity (GR) with the standard matter field in the presence of a quintessence field ϕ, given by the following action ($8\pi G = c = 1$)

$$S = \int d^4x\sqrt{-g}\left(\frac{1}{2}R - \frac{1}{2}\partial_{\mu}\phi\partial^{\mu}\phi - V(\phi)\right) + S_m\,, \tag{1}$$

where ϕ is the field, $V(\phi)$ is the field's potential, S_m corresponds to standard matter, while R is the Ricci scalar. Moreover, it is well known that when we consider an FRWL Universe with

$$ds^2 = -dt^2 + a(t)^2 \sum_{i=1}^{3} \left(dx^i\right)^2 \ , \tag{2}$$

the dynamics of the scalar field's dark energy and dark matter are described by the equations

$$\dot{\rho}_\phi + 3H\left(\rho_\phi + P_\phi\right) = 0 \, , \tag{3}$$

$$\dot{\rho}_{dm} + 3H\rho_{dm} = 0 \ , \tag{4}$$

with

$$H^2 = \frac{1}{3}\left(\rho_\phi + \rho_{dm}\right). \tag{5}$$

In other words, Eqs. (3)-(5) describe the background dynamics. Furthermore, it is well known that ρ_ϕ, ρ_{dm} and $P = P_\phi$ are related to each other through the equation

$$\dot{H} + H = -\frac{1}{6}\left(\rho_\phi + \rho_{dm} + 3P_\phi\right). \tag{6}$$

On the other hand, assuming that the scalar field is spatially homogeneous, for the energy density and pressure we will have

$$\rho_\phi = \frac{1}{2}\dot{\phi} + V(\phi), \tag{7}$$

and

$$P_\phi = \frac{1}{2}\dot{\phi} - V(\phi), \tag{8}$$

where the dot means derivative w.r.t. the cosmic time, while $V(\phi)$ is the potential of the scalar field (see for instance

[43] and references therein for more discussion). In all equations above $H = \dot{a}/a$ is the Hubble parameter. This is well known, and also the important fact that the analysis of the background dynamics requires assuming the form of the potential $V(\phi)$; various forms for it have been considered in the literature.

Anyway, after some simple algebra, one can see that, starting from Eqs. (7) and (8), it turns out that

$$\dot{\phi}^2 = \rho_\phi + P_\phi \,, \tag{9}$$

while

$$V(\phi) = \frac{\rho_\phi - P_\phi}{2}. \tag{10}$$

On the other hand, it is easy to see that from Eq. (4) we have $\rho_{dm} = 3H_0^2\,\Omega_0(1+z)^3$, while from Eq. (5) we can determine the energy density of the scalar field

$$\rho_\phi = 3H^2 - 3H_0^2\,\Omega_0\,(1+z)^3 \,, \tag{11}$$

where H_0 is the value of the Hubble parameter at $z = 0$ (e.g., at present; z is the redshift). On the other hand, Ω_0 is the cold dark matter density fraction at $z = 0$. Now, we can use Eq. (6) and, after some algebra,

$$P_\phi = 2(1+z)HH' - 3H^2 \,, \tag{12}$$

where the prime denotes derivative w.r.t. the redshift. Coming back to Eqs. (9) and (10), we see that Eqs. (11) and (12) allow us to write down the form of the scalar field potential in terms of H and H', as follows

$$V(z) = 3H^2 - H'H(z+1) - \frac{3}{2}H_0^2\,\Omega_0\,(z+1)^3 \,. \tag{13}$$

Moreover, it is possible to see that, for the field itself, we have

$$(\phi(z)')^2 = \frac{2H'H - 3H_0^2\,\Omega_0(z+1)^2}{(1+z)H^2}, \tag{14}$$

what allows to perform an end-to-end reconstruction of $V(\phi)$, provided $H(z)$ and $H'(z)$ are known. It should be noted that in [43] several other further steps have been taken too, in order to study the Swampland criteria; however,

the discussion carried out here and the ensuing results, had never been discussed before.

Now, it is time to make more transparent to the reader how can one obtain a model-independent reconstruction of $V(\phi)$, from Eqs. (13) and (14). It is easy to see, to start, that Eqs. (13) and (14) allow doing this, if model-independent reconstructions of $H(z)$ and $H'(z)$ are provided. Namely, following [43], we choose the GP to reconstruct $H(z)$ and $H'(z)$ from available expansion rate data (see Table 1). Therefore the rest of this section is devoted to the presentation of some crucial aspects of GPs. To start, we recall that GPs are Bayesian state-of-the-art tools and that the key ingredient is the covariance function. In a nutshell, it is assumed that a GP prior governs the set of possible latent functions, and the likelihood of the latent function and observations shape this prior and produce posterior probabilistic estimates. The advantage of a GP is providing a full conditional statistical description of the predictions used to establish confidence intervals and to set hyper-parameters. Moreover, GPs should be understood as distributions over functions, characterized by a mean function and a covariance matrix. Unfortunately, one disadvantage of the method is that the choice of the kernel is not a fixed process. Only well-designed data and the type of task to be tackled can indicate which kernel works better. A number of possible choices for the covariance function exist - as squared exponential, polynomial, spline, etc., to mention a few. In other words, it is always highly recommended to consider several kernels and compare the results obtained, in order to be sure that the reconstruction has not been got by chance. This is very important and not treating this aspect very seriously can lead to misleading results, with bad consequences. In cosmology we deal with relatively small datasets, therefore it is always possible to follow the reconstruction process which significantly reduces the kernel numbers to be considered. This is one of the reasons that in cosmology we usually meet studies involving only two or three kernels. In particular, in cosmology one of the most actively used kernels is the squared exponential function

$$k(x,x')=\sigma_f^2\exp\left(-\frac{(x-x')^2}{2l^2}\right), \tag{15}$$

where σ_f and l are known as hyperparameters. The l parameter represents the correlation length along which the successive $f(x)$ values are correlated, while to control the variation in $f(x)$ relative to the mean of the process we need the σ_f parameter. Recently, other kernels including the so-called Matern ($\nu=9/2$) covariance function

$$k_M(x,x')=\sigma_f^2\exp\left(-\frac{3|x-x'|}{l}\right)$$
$$\times\left[1+\frac{3|x-x'|}{l}+\frac{27(x-x')}{7l^2}+\frac{18|x-x'|^3}{7l^3}+\frac{27(x-x')^4}{35l^4}\right], \tag{16}$$

have been used for different purposes, too. Following this benchmark, we have also considered the squared exponential, Eq. (15), and the Matern ($\nu=9/2$), Eq. (16), which allow eventually to understand 1) how they can affect

TABLE 1. $H(z)$ and its UUncertainty σ_H in Uunits of km s^{-1} Mpc^{-1}

z	$H(z)$	σ_H	z	$H(z)$	σ_H
0.070	69	19.6	0.4783	80.9	9
0.090	69	12	0.480	97	62
0.120	68.6	26.2	0.593	104	13
0.170	83	8	0.680	92	8
0.179	75	4	0.781	105	12
0.199	75	5	0.875	125	17
0.200	72.9	29.6	0.880	90	40
0.270	77	14	0.900	117	23
0.280	88.8	36.6	1.037	154	20
0.352	83	14	1.300	168	17
0.3802	83	13.5	1.363	160	33.6
0.400	95	17	1.4307	177	18
0.4004	77	10.2	1.530	140	14
0.4247	87.1	11.1	1.750	202	40
0.44497	92.8	12.9	1.965	186.5	50.4
0.24	79.69	2.65	0.60	87.9	6.1
0.35	84.4	7	0.73	97.3	7.0
0.43	86.45	3.68	2.30	224	8
0.44	82.6	7.8	2.34	222	7
0.57	92.4	4.5	2.36	226	8

The upper panel of the Table 1 consists of thirty samples deduced from the differential age method. The lower panel corresponds to ten samples obtained from the radial BAO method. The table is according to [42] (see the references therein to find out how each of the data points has been obtained).

the reconstruction of $V(\phi)$, and 2) how it can affect the constraints on $V(\phi)$ potentials existing in the literature. It should be mentioned that we have considered a number of particular cases, but the reconstructions here presented are well enough to revisit all existing models. We will come back to this in the next section when we discuss the results obtained.

Now, having closed the question of the kernel functions, let us discuss 1) the data and 2) the tools we use. In particular, the data used is the expansion rate values presented in Table 1, consisting of 30-point samples of $H(z)$ deduced from the differential age method in addition to 10-point samples obtained from the radial BAO method. In total, we use 40 data points covering the $z \in [0, 2.4]$ redshift range. One interesting aspect of our analysis concerning the value of H_0 at $z = 0$ to be mentioned here is the adopted strategy. To wit, during the reconstruction, we consider

three different cases: 1) H_0 is estimated from the expansion rate data during the reconstruction of $H(z)$ and $H'(z)$, 2) H_0 is taken from the Planck mission and the forms of $H(z)$ and $H'(z)$ are reconstructed, and finally, 3) H_0 is the one from the Hubble mission and then the forms of $H(z)$ and $H'(z)$ are reconstructed. The reason for this, as it can be realized, is to see whether or not it is possible to find ways to solve or at least alleviate the H_0 tension problem.

To end this section we need to mention that we use the publicly available package GaPP (Gaussian Processes in Python) developed by Seikel et al. [54]. It is a very easy one to use and a very friendly package allowing to choose different covariance functions (new ones can be added easily, too). Moreover, the squared exponential function, Eq. (15), is used in the code as a default option, while the Matern covariance function given by Eq. (16), is already implemented. On the other hand, the code is very useful to combine different observational datasets, provided the proper relation between them is known. The package has been often used, and more details about it, including a detailed description of the GP, can be found in the references of our paper. In the next section, we will describe our results thoroughly, which together with the discussion in the above section, will surely allow the readers to understand how the scheme of the reconstruction of the potential of the quintessence dark energy can be extended and applied to the other dark energy models, as phantom or tachyonic models.

3. Results and discussion

In this section, we present and discuss our results. They can be split into three different cases, corresponding to the reconstruction when: 1) H_0 is estimated from a GP, 2) H_0 is fixed to the value estimated from the Planck mission results and the reconstruction of $H(z)$ and $H'(z)$ is performed, and 3) H_0 is fixed to the value estimated from the Hubble mission and then the reconstruction of $H(z)$ and $H'(z)$ is performed. In this way, we can get a hint on when the H_0 tension problem could be solved and what are the constraints on some explicitly given model parameters in that case. We are interested in a model-independent reconstruction of the quintessence dark energy potential and we use the expansion rate data and the GP to reconstruct $H(z)$ and $H'(z)$ in Eqs. (13) and (14). The reconstruction of the functions $H(z)$ and $H'(z)$ for the squared exponential function, Eq. (15), assuming that H_0 = 73.52 ± 1.62 km s^{-1} Mpc^{-1} can be found in Fig.1. The functions $H(z)$ and $H'(z)$ corresponding to other cases can be reconstructed similarly. A crucial point, not discussed in the previous section, is how to deal with Eq. (14) since eventually, we will reconstruct $V(\phi)$. This problem is the simplest one since

$$\phi(z_i)' \approx \frac{\phi(z_i + \Delta z) - \phi(z_i)}{\Delta z}, \tag{17}$$

where $\Delta z = z_{i+1} - z_i$ with z_i correspond to the redshifts where $H(z)$ and $H'(z)$ have been reconstructed. It is clear, that Eqs. (13), (14) and (17) allow to perform the model-independent reconstruction of the potential $V(\phi)$ describing quintessence dark energy in our Universe.

3.1. $V(\phi)$ **reconstruction when** H_0 **is not fixed.** The first case corresponds to the reconstruction when H_0 is not fixed. In this case, using GP and given data, Table 1, we first estimate H_0 during the reconstruction process. It is H_0 = 71.286 ± 3.743 km s^{-1} Mpc^{-1} when the kernel is given by Eq. (15), while when the kernel is given by Eq. (16), we found that H_0 = 71.196 ± 3.867 km s^{-1} Mpc^{-1}. Then using the reconstructed $H(z)$ and $H'(z)$ in Eqs. (13) and (14) (combined with Eq. (17)) we can finish the model-independent reconstruction of $V(\phi)$. Omitting other non-relevant technical details, we refer the reader to Fig.5, which depicts the model-independent reconstructed forms of the potential $V(z)$ and field $\phi(z)$. The reader may have already noted that the estimated errors for H_0 are significantly larger than those from the Planck data and those from the Hubble mission. It should be mentioned that, as a consequence of these upper and lower bounds on $V(\phi)$, this case will significantly differ from the other two cases. In general, this can have a strong impact on the model parameter constraints and affect the viable model selection. Obviously, in general, this can affect the early-time behavior of a given quintessence dark energy model.

We now elaborate on our reconstruction results. At first glance, the reconstruction has been successful. However, to understand and validate the corresponding results, we need to have a look at another physical quantity that has been reconstructed, too. It is important to understand up to what extent we can believe in the model validity in our case. In general, non-validation of the reconstruction results can lead to wrong interpretations and cause misunderstanding of the underlying physics. The physical quantity we choose for this purposes is $\Omega_{de} = \rho_\phi / 3H^2$, which at $z = 0$ has actually been used to estimate ϕ ($z = 0$), too.

The results of the reconstruction of the Ω_ϕ can be found in Fig.6 for both kernels given by Eqs. (15) and (16), respectively. Indeed, we see that the reconstruction was successful up to a certain redshift, indicating that for higher values the model should be rejected since the lower 2σ bound of Ω_{de} is negative. It is important to mention that the GP gives the statistical explanation of the results, and considering only the means to decide whether or not

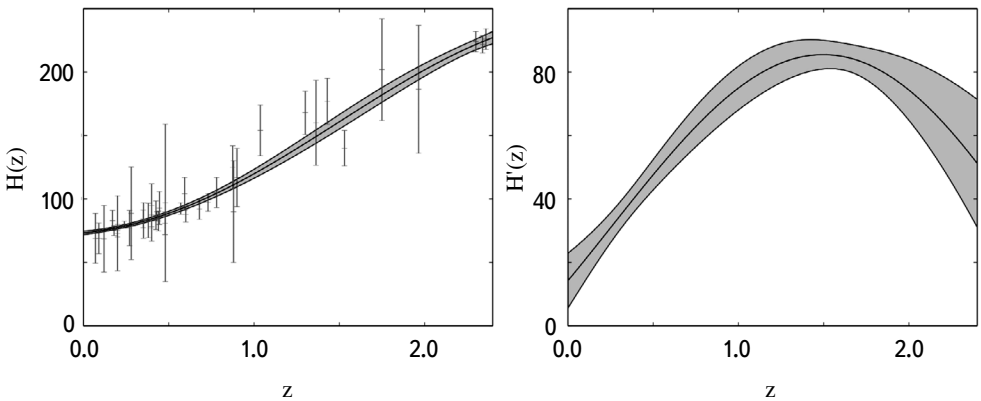

Fig.1. GP reconstruction of $H(z)$ and $H'(z)$ for the 40-point sample deduced from the differential age method, with the additional 10-point sample obtained from the radial BAO method, when H_0 = 73.52 ± 1.62 km s^{-1} Mpc^{-1} reported by the Hubble mission. The $'$ means derivative with respect to the redshift z.

something is working is not a correct procedure. To have a proper understanding, we need to consider the whole picture, which in our case indicates that the reconstruction of $V(z)$ and $\phi(z)$ is acceptable up to some redshift. Having this in mind, we continued the study and, using the means of the reconstructed $V(z)$ and $\phi(z)$, we have directly reconstructed the mean of $V(\phi)$.

On the other hand, using the lower and upper 2σ error bounds of both the $V(z)$ and $\phi(z)$ reconstructed functions, we have determined possible maximum errors for $V(\phi)$ allowing to complete our task, which was to obtain a model- independent reconstruction of $V(\phi)$ describing quintessence dark energy as the driving force of our expanding Universe. The result can be found in Fig.2, where the left-hand side plot represents the reconstruction result when the kernel is given by Eq. (15), while the right-hand side one stands for the case with kernel given by Eq. (16), respectively.

Fig.2 shows how different models can be compared and constrained using the reconstruction. In particular, we see why the quintessence dark energy model with $V(\phi) \sim e^{-\lambda\phi}$ (dashed curve, for instance, with $\lambda = 0.854$ in the left-hand side plot of Fig.2, is among the most successful ones. Our analysis explains why this particular model has captured such a lot of attention in the literature. On the other hand, we also see that the quintessence dark energy model with $V(\phi) \sim \phi^{\lambda}\left[1-\cos\left(\beta\phi^{n}\right)\right]$ (solid curve with $\beta = 1.65$, n = 0.05 and $\lambda = 0.2$, for instance) will not work very well and there is a hint that it should be rejected. Additionally, the model with potential $V(\phi) \sim \phi^{\lambda}$ (dotted curve with $\lambda = 0.125$) should be kept, and it will work better than the model with $V(\phi) \sim \phi^{\lambda}\left[1-\cos\left(\beta\phi^{n}\right)\right]$. This is inferred from the curves on both plots of Fig.2.

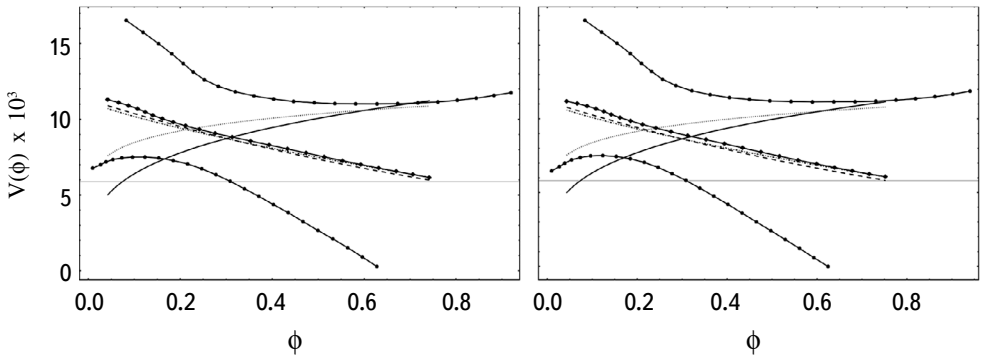

Fig.2. Reconstructed $V(\phi)$ for the case when H_0 = 71.286 ± 3.743 km s^{-1} Mpc^{-1} has been estimated by a GP using the expansion rate data presented in Table 1. The curve with black squares corresponds to the mean of the reconstructed $V(\phi)$ model obtained from the reconstructed means of the functions $V(z)$ and $\phi(z)$. The lower and upper 2σ error bounds of both reconstructed functions $V(z)$ and $\phi(z)$ have been used to determine possible maximum error bounds for $V(\phi)$ (curves with black circles).

It is made clear from the provided discussion that any given model can be analyzed, and that proper constraints on the parameters can be found. Going one step further, it should be now possible to see why some dark energy models with specific potentials will not work for solving the H_0 tension problem. Moreover, in the next subsection, we will discuss how drastically the constraints on the model parameters should be changed to be suitable to solve the H_0 tension problem.

Before ending this one, and based on the reconstructed results, we suggest a new form for the potential to describe a viable quintessence dark energy model. From what we know, this specific model has not been considered before. The potential has the form

$$V(\phi) \sim \phi^{\lambda}\left[1-\sin^{n}(\beta\phi)\right], \tag{18}$$

where λ, n, and β are free parameters to be fitted. The dot-dashed black curve of Fig.2 corresponds to this model; it is one-to-one in mimicking the reconstructed mean behavior with $\lambda = 0.001$, $\beta = 0.5$ and $n = 0.5$, when the kernel is given by Eq. (15). To finish, we should mention that the consideration of the kernel, Eq. (16), will introduce changes only slightly affecting the above-discussed numerical values of the parameters. However, the general picture and the conclusions drawn remain unchanged.

3.2. $V(\phi)$ reconstruction when H_0 = 67.40 ± 0.5 km s^{-1} Mpc^{-1}. In this subsection, we discuss the case when a specific value for H_0 has been fixed in advance and used in the reconstruction. Different from the previous case, now the reconstruction is based on 41 data points. We will later see that this can affect our perception of the situation and can be moreover useful to understand why the constraints on quintessence dark energy models discussed in the recent literature may be so different. To be more precise let us indicate that we use the H_0 reported by the Planck mission. Similar to the previous case, $\Omega_{de} = \rho_{\phi}/3H^2$ has been considered again allowing us to determine the redshift range where the reconstruction is valid. In particular, we found that when the squared exponent kernel given by Eq. (15) is considered then the $z \in [0, 2)$ redshift range provides a physically acceptable reconstruction of the functions $V(z)$ and $\phi(z)$. Moreover, when we consider the Matern ($\nu = 9/2$) kernel, Eq. (16), then $z \in [0, 1.91)$ is the redshift range providing physically acceptable reconstructions of $V(z)$ and $\phi(z)$ (see Fig.8). On the other hand, from the top panel of Fig.7 we realize the reconstructed forms of the potential $V(z)$ and the field $\phi(z)$, when the kernel is given by Eq. (15). Complementary, the reconstruction results when the kernel is given by Eq. (16) can be found on the bottom panel of Fig.7.

To reconstruct the mean of $V(\phi)$ potential we have used the means of the reconstructed $V(z)$ and $\phi(z)$. Moreover, using the lower and upper 2σ error bounds of both reconstructed functions, $V(z)$ and $\phi(z)$, we have determined possible maximal errors for $V(\phi)$ (Fig.3), what allowed us to complete the model-independent reconstruction of the $V(\phi)$ describing the quintessence dark energy in our expanding Universe. The reconstruction results can be found in Fig.3, where the left-hand side plot represents the reconstruction result when the kernel is given by

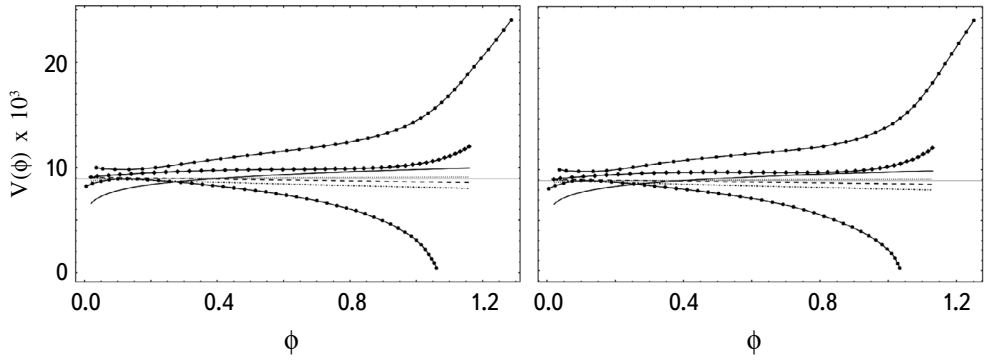

Fig.3. Reconstructed $V(\phi)$ for the expansion rate data in Table 1 with H_0= 67.40±0.5 km s^{-1}Mpc^{-1}. The curve with black squares corresponds to the mean of the reconstructed $V(\phi)$ model obtained from the reconstructed means of the functions $V(z)$ and $\phi(z)$. The lower and upper 2σ error bounds of both reconstructed functions $V(z)$ and $\phi(z)$ have been used to determine possible maximum error bounds for $V(\phi)$ (curves with black circles). The dashed curve represents the quintessence dark energy model with potential $V(\phi) \sim e^{-\lambda\phi}$. The dotted, dot-dashed, and solid curves correspond to the quintessence dark energy model with $V(\phi) \sim \phi^{\lambda}$, $V(\phi) \sim \phi^{\lambda}[1-\sin^{n}(\beta\phi)]$ and $V(\phi) \sim \phi^{\lambda}[1-\cos(\beta\phi^{n})]$, respectively. The left-hand side plot is the result of the reconstruction when the kernel is given by Eq. (15), while the right-hand side one stands for the case with kernel given by Eq. (16).

Eq.(15), while the right-hand side one corresponds to the case with kernel given by Eq.(16).

Visual comparison of the results presented in Fig.2 and Fig.3 already points out huge differences. In particular, just comparing the mean of the reconstruction with $V(\phi) \sim e^{-\lambda\phi}$, we conclude that the model with $\lambda = 0.05$ should be preferred for cosmological applications. On the other hand, with $\lambda = 0.01$ the model with the potential $V(\phi) \sim \phi^{\lambda}$ may be highly recommended for doing cosmology. Moreover, we also conclude that, with $\beta = 0.05$, n = 0.75 and $\lambda = 0.001$, the model with potential $V(\phi) \sim \phi^{\lambda}\left[1-\sin^{n}(\beta\phi)\right]$ is favored for doing cosmology. Finally, the model with $V(\phi) \sim \phi^{\lambda}\left[1-\cos\left(\beta\phi^{n}\right)\right]$ can be recommended too, if $\lambda = 0.02$, $\beta = 1.65$ and n = 0.05.

In all these examples, the kernel was given by Eq. (15). Our analysis using the kernel of Eq. (16) shows that similar recommendations can be made. However, we should note that the reconstruction indicates that here we will have tighter constraints on the model parameters than in the previous case. However, the most relevant aspect revealed from the reconstruction is that the early time behavior of the models can change significantly. This is a hint indicating that the H_0 tension is not just a result of playing with numbers. It is more profound than this, namely a problem related to physics and corresponding considerations. This should be made more clear in the next subsection, where we will present the results corresponding to the reconstruction based on the value of H_0 reported by the Hubble mission.

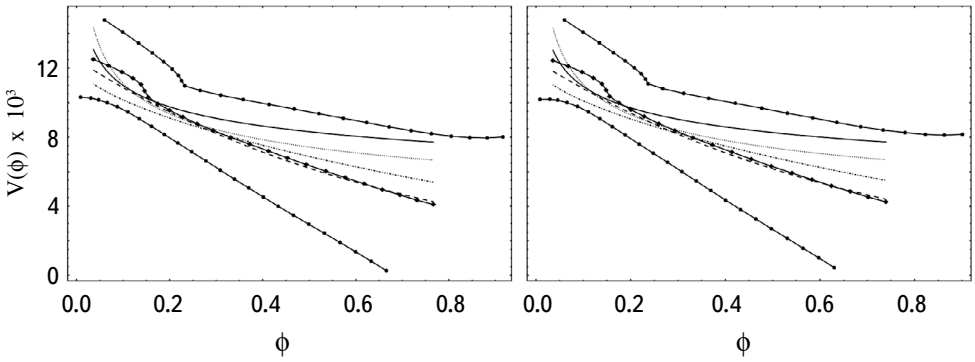

Fig.4. Same as Fig.3, but with H_0 = 73.52 ± 1.62 km s^{-1} Mpc^{-1}.

3.3. $V(\phi)$ **reconstruction when** H_0 **= 73.52 ± 1.62 km s^{-1} Mpc^{-1}.** The last case to be discussed here is when H_0 is fixed to the value H_0 = 73.52 ± 1.62 km s^{-1} Mpc^{-1} reported by the Hubble mission. This means that similarly to the second case, the reconstruction of $H(z)$ and $H'(z)$ will be also based on 41 data points. The reconstructed $V(z)$ and $\phi(z)$ for $z \in [0, 2.4]$ can be found in Fig.9. The reconstruction there has been obtained for the squared exponent kernel given by Eq. (15). The final results of the reconstruction are depicted in Fig.4.

Our analysis based on these reconstructions shows when the resulting potentials can be recommended for cosmology. In particular, we found that according to the mean of the $V(\phi)$ reconstruction, the model with $V(\phi) \sim e^{-\lambda\phi}$ and $\lambda = 1.4$ is expected to be useful for cosmological applications. On the other hand, the model with potential $V(\phi) \sim \phi^{\lambda}$ can be highly recommended, provided $\lambda = -0.25$. Moreover, we found also that, with $\beta = 0.5$, n = 0.576 and $\lambda = 0.005$, the model with potential $V(\phi) \sim \phi^{\lambda}\left[1 - \sin^{n}(\beta\phi)\right]$ is also favored for cosmological applications. Finally, the model with $V(\phi) \sim \phi^{\lambda}\left[1 - \cos\left(\beta\phi^{n}\right)\right]$ is also useful, provided $\lambda = -0.25$, $\beta = 1.75$ and n = 0.05. In all these examples the kernel was given by Eq. (15). An analysis using the kernel of Eq. (16) shows that similar recommendations can be done, too. Moreover, the reconstruction results indicate that here the constraints on the model parameters will not be tighter than in the case discussed in Sect. 3.2. On the other hand, the early time behavior of the models could change significantly. The reconstruction of the $\Omega_{de} = \rho_{\phi}/3H^2$ has been considered again allowing us to determine the redshift range where the reconstruction is valid (Fig.10).

To end this subsection let us mention that the values of the parameters for the models presented above give a hint on when the H_0 tension problem can be solved, in a quintessence dark energy-dominated Universe, when one of the forms for the potential discussed above is used. Let us mention again that reconstructions here obtained are model-independent and based on the expansion rate data, and that they can be used either to craft new models or to constrain already existing ones.

4. Conclusions

In this paper, we have used GPs and available expansion rate data to reconstruct the functional form of the potential better-representing quintessence dark energy. There are various and important open questions about dark energy physics and the challenge of answering them is usually undertaken using model-dependent approaches. The quintessence dark energy paradigm is among the most often discussed models. In there, the form of the potential field is chosen manually, in a sort of phenomenological approach, mainly aimed at reproducing the observational data. We notice that the same is true for other dark energy models and that mainly phenomenology-based motivations have been put forward to craft viable dark energy models.

As an alternative to all these previously carried out studies, we describe in detail the whereabouts of a model-independent reconstruction of the potential. Moreover, the results of the reconstruction can be used to build new potentials and to constrain the free parameters. Starting from very basic assumptions about the background dynamics, we have demonstrated that the potential and the field itself can be expressed in terms of $H(z)$ and $H'(z)$, which can be reconstructed in a model-independent way from the expansion rate data using a GP. GPs are among several very useful Machine Learning tools intensively used in very different areas, among them in cosmology.

The main issue with this approach is to specify the form of the kernel function that needs to be chosen to be able to complete the reconstruction. The literature contains various interesting discussions indicating that it is better to use several kernels and compare the results. This is, in our opinion, an optimal solution that can be time-consuming; however, it is judicious to follow this approach and make sure that the hints and the results obtained have value and have not been obtained by chance.

In our work, the quintessence dark energy potential and the corresponding field have been reconstructed for three different cases: 1) when H_0 has been estimated from the GP reconstruction of the functions $H(z)$ and $H'(z)$, based on an existing 40-point expansion rate dataset; 2) when H_0 is fixed to the value estimated from the Planck mission and then the reconstruction of $H(z)$ and $H'(z)$ is performed; 3) when H_0 is fixed to the value estimated from the Hubble mission results and then the reconstruction of $H(z)$ and $H'(z)$ is performed. In this way, we get a hint on when the H_0 tension problem could be reasonably solved, for instance, when the model with $V(\phi) \sim e^{-\lambda\phi}$ is considered. We have studied other models, too, and also found a new potential, $V(\phi) \sim \phi^{\lambda}\left[1-\sin^{n}(\beta\phi)\right]$, which can be recommended to be used in cosmology. This is a genuine discovery made in this paper. An in-depth study of this new potential has been left for future publication.

We need to mention that, in our analysis, we have used the two kernel functions given by Eqs. (15) and (16), and found slight changes (detailed above), as compared with the results discussed before, but those are not so important. However, we would like to discuss another result we have at this point. First, concerning the possible constraints on the λ parameter of the Swampland $V(\phi) \sim e^{-\lambda\phi}$ potential, which was discussed in [55]. Without going deep into the discussion of [55], we learned that, with future surveys, we should expect fundamental observational limitations, λ to $\lambda < 0.1$, supporting the standard model. Now the question is: what we have learned with our method? To understand this, let us summarize what we obtained, namely the preferred values for the parameters: 1)

$\lambda = 0.854$ when H_0 is not fixed, 2) $\lambda = 0.01$ when H_0 = 67.40 ± 0.5 km s^{-1} Mpc^{-1}, and finally 3) when H_0 = 73.52 ± 1.62 km s^{-1} Mpc^{-1} we got $\lambda = 1.4$. In all cases, we have just used the reconstruction means, and the last one means that, if we use lower error bounds of the reconstruction, we will reduce the estimated values too.

Anyhow, the important message we wish to transmit to the reader is 1) that the 40 data point expansion rate data already contains the information that can come from future surveys; 2) the great importance of the tool we use to extract information from data. Moreover, our constraints on the parameter λ when H_0 = 67.40 ± 0.5 km s^{-1} Mpc^{-1} indicate that any other estimation closer to the estimation obtained here definitely supports the ΛCDM standard model. In all other cases, we can claim that the ΛCDM theory might be challenged. This is an indication that the H_0 tension problem is not a game of statistics only.

Of course, there are other various questions to be studied yet, which have been left for further consideration. In particular, to continue using GPs and other Machine Learning algorithms involving other datasets for model-independent reconstruction or pattern learning that can be used for similar estimations and reconstructions. More specifically, it would be interesting to see if the recently discovered constraints would be challenged in those cases, and what the consequences of this could be.

Acknowledgements

The authors would like to thank the referee for valuable comments which helped to improve the manuscript. We thank Eoin O Colgain, Reginald Christian Bernardo, and Carlos Garcia-Garcia for their valuable comments and discussion. Here, we need to mention that we learned about [51] after our recent paper appeared online. This work has been partially supported by MICINN (Spain), project PID2019-104397GB-I00, of the Spanish State Research Agency program AEI/10.13039/501100011033, by the Catalan Government, AGAUR project 2017-SGR-247, and by the program Unidad de Excelencia María de Maeztu CEX2020-001058-M. This work has been supported by the Juan de la Cierva-incorporación grant (IJC2020-042690-I). This paper was supported by the Ministry of Education and Science of the Republic of Kazakhstan, grant AP08052034.

APPENDIX

We include here several additional figures, Fig.5-10, to allow the reader to estimate the quality of the reconstructions presented in the paper.

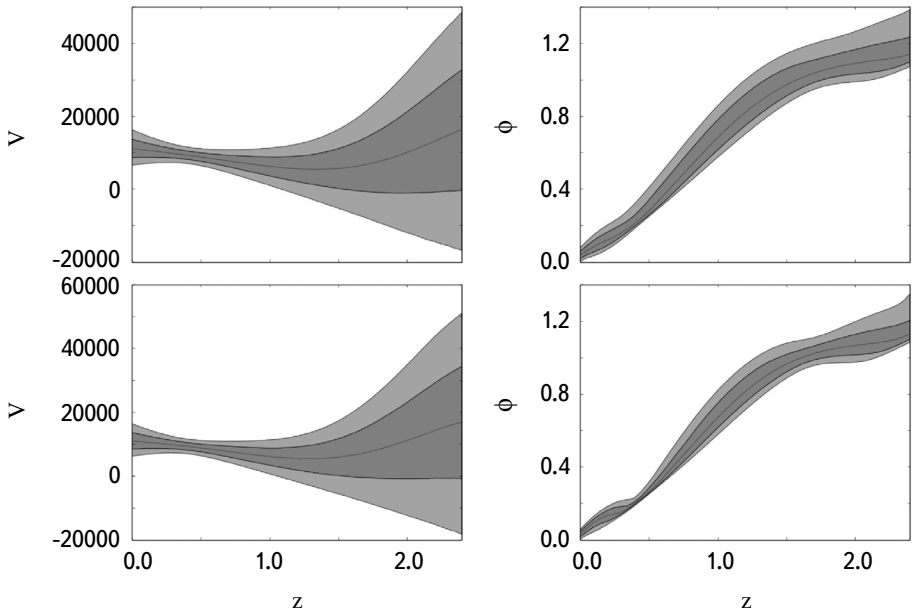

Fig.5. Reconstruction of $V(z)$, Eq. (13), and $\phi(z)$, Eq. (14), from the $H(z)$ data depicted in Table 1. The plots of the top panel correspond to the GP reconstruction for the squared exponent kernel given by Eq. (15). The plots of the bottom panel correspond to the GP reconstruction for Matern ($\nu = 9/2$) kernel given by Eq. (16). The solid line is the mean of the reconstruction and the shaded regions are the 68% and 95% C.L. of the reconstruction, respectively. H_0 = 71.286 ± 3.743 km s^{-1} Mpc^{-1} and $H_0 = 71.196 \pm 3.867$ km s^{-1} Mpc^{-1} estimates for H_0 have been obtained using GP when the kernels are given by Eq. (15) and Eq. (16), respectively.

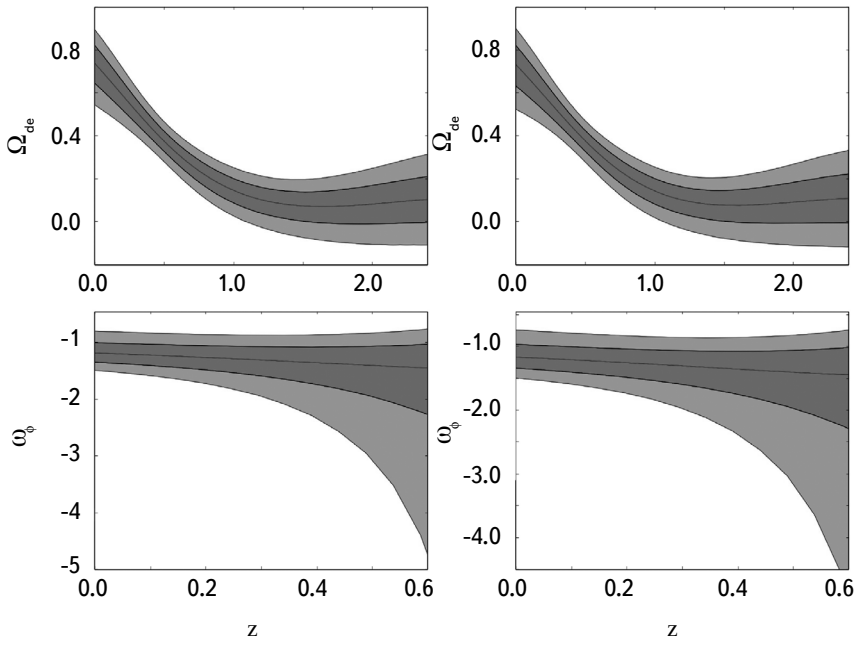

Fig.6. The top panel represents the reconstruction of $\Omega_{de} = \rho_\phi / 3H^2$ from the $H(z)$ data depicted in Table 1. The left-hand side plot corresponds to the GP reconstruction for the squared exponent kernel given by Eq. (15). The right-hand side plot corresponds to the GP reconstruction for the Matern ($\nu = 9/2$) kernel given by Eq. (16). The solid line is the mean of the reconstruction and the shaded regions are the 68% and 95% C.L. of the reconstruction, respectively. H_0 = 71.286 ± 3.743 km s^{-1} Mpc^{-1} has been estimated by GP from the data presented in Table 1 when the squared exponent kernel given by Eq. (15) has been used. On the other hand, H_0 = 71.196 ± 3.867 km s^{-1} Mpc^{-1} has been estimated by GP from the data presented in Table 1 when the Matern ($\nu = 9/2$) kernel given by Eq. (16) has been used. The bottom panel represents the reconstruction of $\omega_\phi = P_\phi / \rho_\phi$ where P_ϕ and ρ_ϕ are given by Eq. (12) and Eq. (11), respectively, while $\Omega_0 = 3.15 \pm 0.007$.

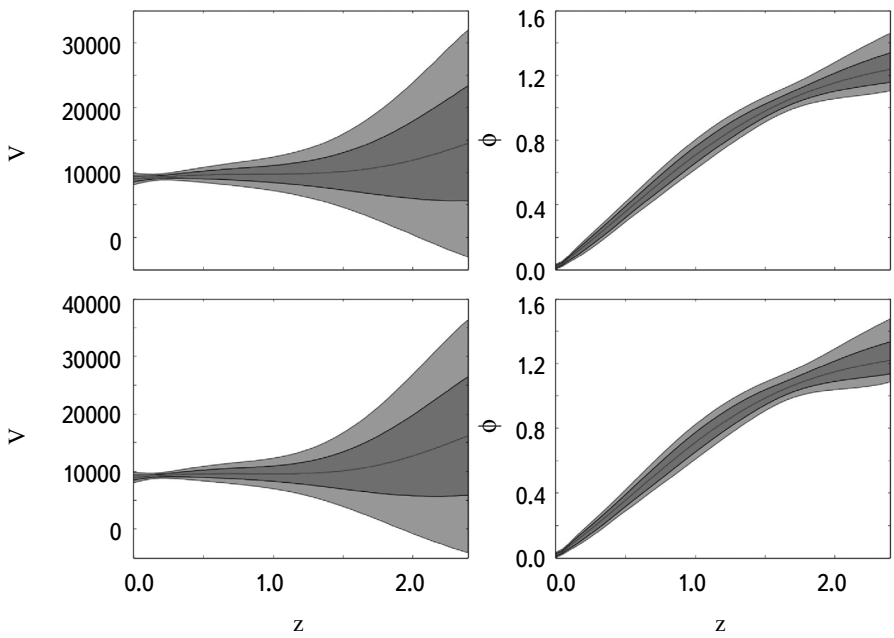

Fig.7. Reconstruction of $V(z)$, Eq. (13), and $\phi(z)$, Eq. (14), from the $H(z)$ data depicted in Table 1 when $H_0 = 67.40 \pm 0.5$ km s^{-1} Mpc^{-1}. The plots of the top panel correspond to the GP reconstruction for the squared exponent kernel, Eq. (15). The plots of the bottom panel correspond to the GP reconstruction for the kernel given by Eq. (15). The solid line is the mean of the reconstruction and the shaded regions are the 68% and 95% C.L. of the reconstruction, respectively.

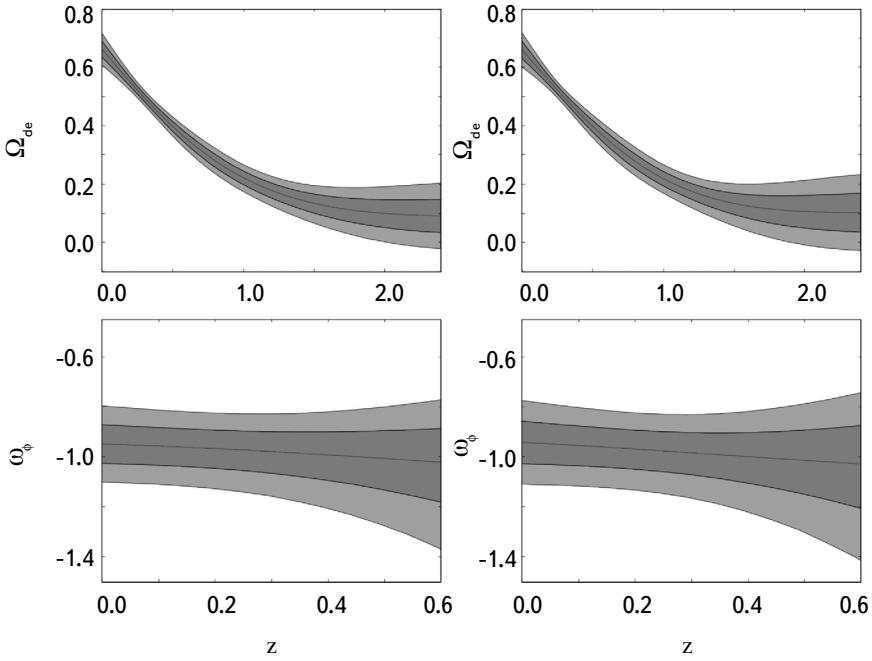

Fig.8. The top panel represents the reconstruction of $\Omega_{de} = \rho_\phi / 3H^2$ from the $H(z)$ data depicted in Table 1 when H_0 = 67.40 ± 0.5 km s^{-1} Mpc^{-1}. The left-hand side plot corresponds to the GP reconstruction for the squared exponent kernel given by Eq. (15). The right-hand side plot corresponds to the GP reconstruction for the Matern ($\nu = 9/2$) kernel given by Eq. (16). The solid line is the mean of the reconstruction and the shaded regions are the 68% and 95% C.L. of the reconstruction, respectively. The bottom panel represents the reconstruction of $\omega_\phi = P_\phi / \rho_\phi$ where P_ϕ and ρ_ϕ are given by Eq. (12) and Eq. (11), respectively, while $\Omega_0 = 3.15 \pm 0.007$.

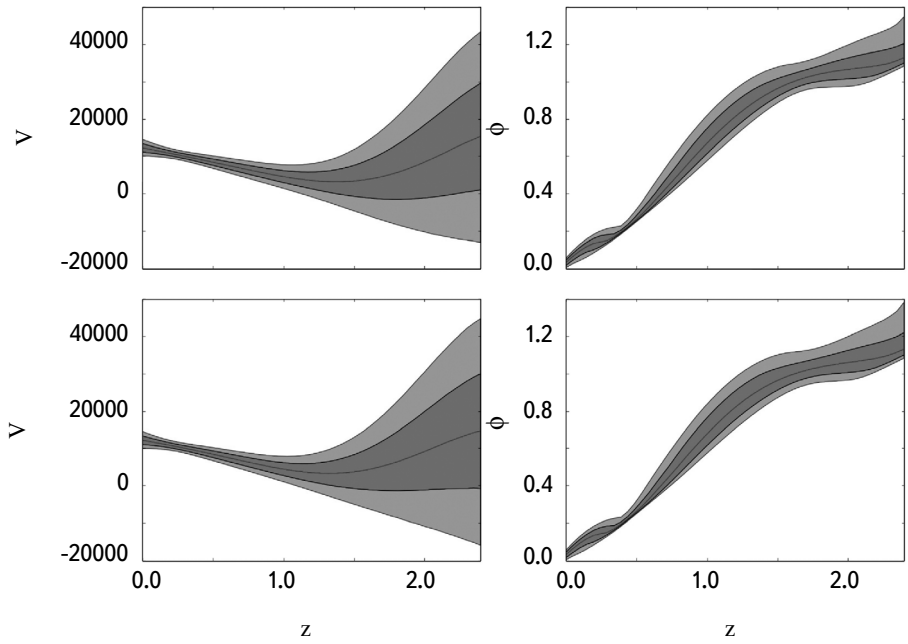

Fig.9. Reconstruction of $V(z)$, Eq. (13), and $\phi(z)$, Eq. (14), from the $H(z)$ data depicted in Table 1 when $H_0 = 73.52 \pm 1.62$ km s^{-1} Mpc^{-1}. The plots of the top panel correspond to the GP reconstruction for the squared exponent kernel, Eq. (15). The plots of the bottom panel correspond to the GP reconstruction for the kernel given by Eq. (15). The solid line is the mean of the reconstruction and the shaded regions are the 68% and 95% C.L. of the reconstruction, respectively.

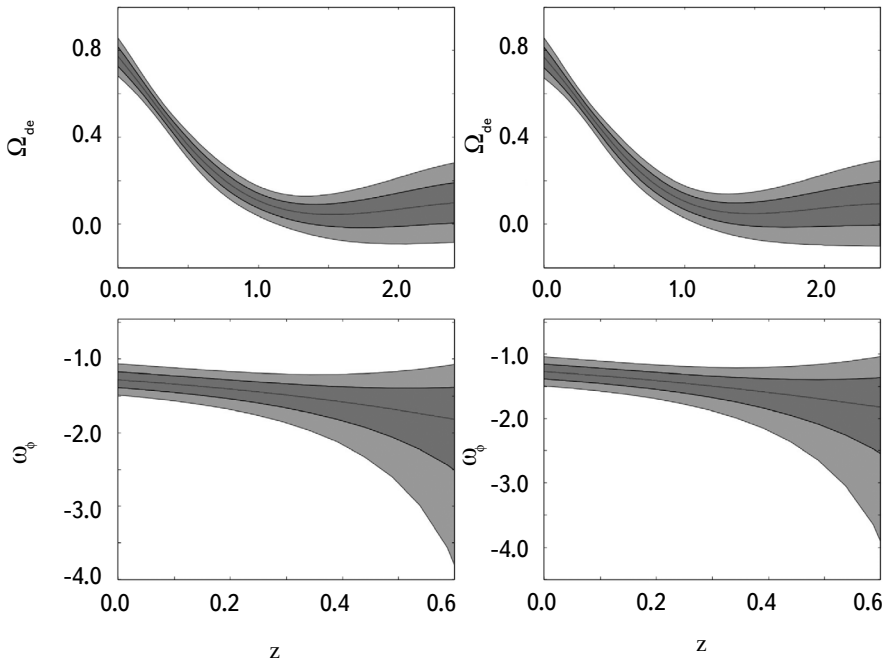

Fig.10. The top panel represents the reconstruction of $\Omega_{de} = \rho_\phi / 3H^2$ from the $H(z)$ data depicted in Table 1, when $H_0 = 73.52 \pm 1.62$ km s^{-1} Mpc^{-1}. The left-hand side plot corresponds to the GP reconstruction for the squared exponent kernel given by Eq. (15). The right-hand side plot corresponds to the GP reconstruction for the Matern ($\nu = 9/2$) kernel given by Eq.(16). The solid line is the mean of the reconstruction and the shaded regions are the 68% and 95% C.L. of the reconstruction, respectively. The bottom panel represents the reconstruction of $\omega_\phi = P_\phi / \rho_\phi$ where P_ϕ and ρ_ϕ are given by Eq. (12) and Eq. (11), respectively, while $\Omega_0 = 3.15 \pm 0.007$.

REFERENCES

1. N. Aghanim et al., Astron. Astrophys., **641**, A6, 2020.
2. A. G. Riess et al., Astrophys. J., **861**(2), 126, 2018.
3. G. S. Sharov, E. S. Sinyakov, arxiv:2002. 03599.
4. E. Elizalde et al., arXiv:2104. 01077.
5. M. Braglia et al., arxiv:2004. 1116.
6. W. L. Kimmy Wu et al., arxiv: 2004. 10207.
7. G. Alestas et al., arxiv:2004. 08363.
8. D. Wang, D. Mota, arxiv:2003. 10095.
9. J. Sakstein, M. Trodden, Phys. Rev. Lett., **124**, 161301, 2020.
10. E. Elizalde et al., arXiv:2006. 12913.
11. E. Elizalde et al., Phys. Rev. D, **102**, 123501, 2020.
12. M. H. P. M. van Putten, arxiv:1707. 02588.
13. E. Di Valentino et al., Phys. Rev. D, **101**, 063502, 2020.
14. M. Khurshudyan, Astrophysics, **66**(3), 423, 2023.
15. S. Nojiri et al., Astrophysics, **65**(4), 534, 2022.
16. R. C. Nunes, JCAP, **05**, 052, 2018.
17. K. Bamba et al., Astrophys. Space Sci., **342**, 155, 2012.
18. S. D. Odintsov et al., Phys. Rev. D, **96**, 044022, 2017.
19. W. Yang et al., arXiv:2001. 02180.
20. W. Yang et al., JCAP, **1911**, 044, 2019.
21. W. Yang et al., JCAP, **1911**, 044, 2019.
22. C. Li et al., Phys. Lett. B, **80**, 135141, 2020.
23. M. Khurshudyan, R. Myrzakulov, Eur. Phys. J. C, **77**, 65, 2017.
24. W. Yang et al., Phys. Rev. D, **99**, 043543, 2019.
25. E. Elizalde, M. Khurshudyan, Int. J. Mod. Phys. D, **27**, 1850037, 2018.
26. E. Sadri et al., Eur. Phys. J. C, **80**, 393, 2020.
27. I. Brevik et al., Int. J. Geom. Meth. Mod. Phys., **14**, 1750185, 2017.
28. S. Capozziello et al., Phys. Rev. D, **73**, 043512, 2006.
29. S. Capozziello et al., Phys. Rev. D, **99**, 023532, 2019.
30. S. Nojiri, S. D. Odintsov, Phys. Rev. D, **72**, 023003, 2005.
31. I. Brevik et al., Phys. Rev. D, **86**, 063007, 2012.
32. I. Brevik et al., Int. J. Mod. Phys. D, **26**, 1730024, 2017.
33. B. Mishra et al., Eur. Phys. J. C, **79**, 34, 2019.
34. S. D. Odintsov et al., Annals Phys., **398**, 238, 2018.

35. K. Yerzhanov et al., Mod. Phys. Lett. A, **36**, 2150222, 2021.
36. M. Aljaf et al., arXiv:2010. 05278.
37. M. Khurshudyan, Symmetry, **10**, 577, 2018.
38. S. Nojiri et al., Phys. Lett. B, **825**, 136844, 2022.
39. S. D. Odintsov et al., Phys. Rev. D, **101**, 044010, 2020.
40. M. Khurshudyan, Int. Journal of Theor. Phys., **53**, 2370, 2014.
41. L. A. Urena-Lopez, N. Roy, Phys. Rev. D, **102**, 063510, 2020.
42. YF. Cai et al., Astrophys. J., **888**, 62, 2020.
43. E. Elizalde, M. Khurshudyan, Phys. Rev. D, **99**, 103533, 2019.
44. M. Aljaf et al., Eur. Phys. J. C, **81**, 544, 2021.
45. E. Elizalde et al., Int. J. Mod. Phys. D, **28**, 1950019, 2018.
46. X. Rin et al., arxiv: 2203. 01926.
47. J. L. Said et al., JCAP, **06**, 015, 2021.
48. A. Gomez-Valent, L. Amendola, JCAP, **1804**, 051, 2018.
49. S. Dhawan et al., Mon. Not. Roy. Astron. Soc., **506**, L1, 2021.
50. E. O. Colgain, M. M. Sheikh-Jabbari, arXiv:2101. 08565.
51. R. C. Bernardo, J. L. Said, JCAP, **09**, 014, 2021.
52. R. C. Bernardo, J. L. Said, JCAP, **08**, 027, 2021.
53. L. O. Tellez-Tovar, T. Matos, J. A. Vázquez, Phys. Rev. D, **106**, 123501, 2022.
54. M. Seikel, C. Clarkson, M. Smith, JCAP, **06**, 036, 2012.
55. L. Heisenberg et al., Phys. Rev. D, **98**, 123502, 2018.